2015

Structural and optical properties of cobalt slanted nanopillars conformally coated with few-layer graphene

Peter M. Wilson
University of Nebraska—Lincoln

Alexey Lipatov
University of Nebraska-Lincoln, alipatov@unl.edu

Daniel Schmidt
University of Nebraska—Lincoln

Eva Schubert
University of Nebraska—Lincoln, efranke3@unl.edu

Mathias Schubert
University of Nebraska—Lincoln, mschubert4@unl.edu

See next page for additional authors

Structural and optical properties of cobalt slanted nanopillars conformally coated with few-layer graphene

Peter M. Wilson,[1] Alexey Lipatov,[1] Daniel Schmidt,[2,3,a)] Eva Schubert,[2,3,4] Mathias Schubert,[2,3,4] Alexander Sinitskii,[1,3,4,b)] and Tino Hofmann[2,3,4,b)]
[1]*Department of Chemistry, University of Nebraska—Lincoln, Lincoln, Nebraska 68588, USA*
[2]*Department of Electrical and Computer Engineering, University of Nebraska—Lincoln, Lincoln, Nebraska 68588, USA*
[3]*Center for Nanohybrid Functional Materials, University of Nebraska—Lincoln, Lincoln, Nebraska 68588, USA*
[4]*Nebraska Center for Materials and Nanoscience, University of Nebraska—Lincoln, Lincoln, Nebraska 68588, USA*

(Received 27 April 2015; accepted 25 May 2015; published online 8 June 2015)

Optical characterization of anisotropic multicomponent nanostructures is generally not a trivial task, since the relation between a material's structural properties and its permittivity tensor is nonlinear. In this regard, an array of slanted cobalt nanopillars that are conformally coated with few-layer graphene is a particularly challenging object for optical characterization, as it has a complex anisotropic geometry and comprises several materials with different topologies and filling fractions. Normally, a detailed characterization of such complex nanostructures would require a combination of several microscopic and spectroscopic techniques. In this letter, we demonstrate that the important structural parameters of these graphene-coated sculptured thin films can be determined using a fast and simple generalized spectroscopic ellipsometry test combined with an anisotropic Bruggeman effective medium approximation. The graphene coverage as well as structural parameters of nanostructured thin films agree excellently with electron microscopy and Raman spectroscopy observations. The demonstrated optical approach may also be applied to the characterization of other nanostructured materials. © *2015 AIP Publishing LLC*.
[http://dx.doi.org/10.1063/1.4922199]

Metallic sculptured columnar thin films (SCTFs) provide a versatile platform for highly sensitive optical sensors based on birefringence changes upon analyte adsorption within the nanostructures.[1,2] The functionalization and stabilization of such three-dimensional (3D) nanostructured surfaces using conformal surface coatings offer interesting practical applications. Graphene, a two-dimensional (2D) carbon allotrope that is known for its excellent mechanical properties[3,4] and its ability to form protective corrosion-inhibiting barriers on metals,[5,6] would be an excellent candidate if a coating of the 3D nanostructured surface can be achieved. In addition, a graphene coating on SCTFs would provide an avenue for chemical functionalization, for example, via diazonium chemistry,[7,8] which could be used to increase the selectivity of the SCTFs to analytes of interest. The investigation of graphene deposited on metallic SCTFs therefore is of high interest. However, in order to fully characterize these graphene-coated materials, several different imaging and optical techniques must typically be used. Since the optical response of the material is a function of many of its structural and material parameters, optical characterization could simultaneously elucidate many of the material's properties. However, optical characterization of complicated anisotropic materials is not simple, since the relation between the material's optical response and its physical and structural properties is intricate. Often, optical characterization of these materials requires the use of complex mathematical models fitted to match experimental data. Thus, to date, no reports describing the optical and structural properties of graphene-coated SCTFs exist in the literature. In this letter, we demonstrate this principle by the fabrication of highly spatially coherent 3D metal nanostructures coated with multilayer graphene using a chemical vapor deposition (CVD) process. The quality of the graphene coating is inspected using confocal Raman microscopy and transmission electron microscopy (TEM), while the optical and structural properties of the nanostructured thin film are investigated using scanning electron microscopy (SEM) and generalized spectroscopic ellipsometry (GSE).[9–13] It is demonstrated that an augmented anisotropic Bruggeman effective medium approximation (AB-EMA) provides an accurate description of the anisotropic optical response of the SCTF, which changes its birefringence behavior from biaxial to uniaxial upon structural variation by slanting angle change incurred upon coating with a conformal graphene layer. The AB-EMA further allows for the determination of the thickness of the conformal graphene coating over each nanopillar. The structural parameters obtained from SEM, TEM, Raman spectroscopy, and through the AB-EMA-based analysis are in good agreement. We conclude that the CVD process leads to a conformal graphene coating of the 3D structures with thickness corresponding to 12–13 graphene monolayers.

Cobalt slanted columnar thin films (SCTFs) were fabricated by electron-beam glancing angle deposition (GLAD) in a custom-built ultra-high vacuum chamber at room

[a)]Present address: Singapore Synchrotron Light Source, National University of Singapore, 5 Research Link, Singapore 117603, Singapore.
[b)]Electronic addresses: sinitskii@unl.edu and thofmann@engr.unl.edu

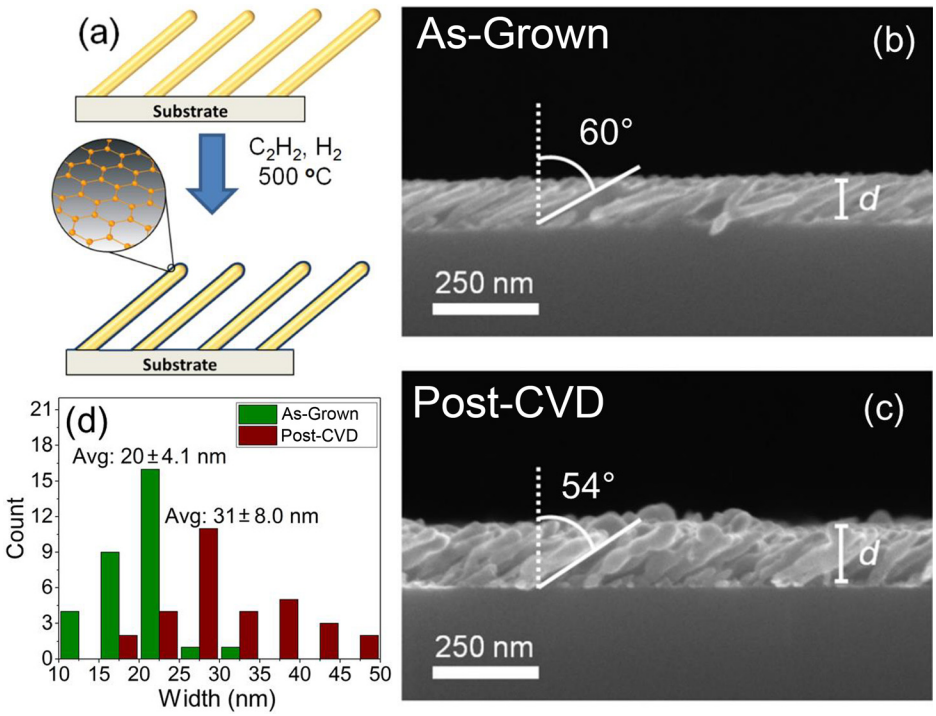

FIG. 1. (a) A schematic of the fabrication of graphene-coated SCTFs. (b) and (c) High-resolution cross-section SEM micrographs obtained from the Co SCTF sample (b) before and (c) after the CVD demonstrate that the 3D nanostructured geometry of the film remains intact after the CVD process. The best-model thickness for the film obtained by GSE is indicated as d (see also Table I). During the CVD growth, the slanting angle slightly decreases from 60.0° to 54.2° while the nanorod length remains constant. (d) Width distribution of pillars before and after CVD.

temperature. The nanocolumnar structures were deposited onto a low-doped n-type (001) silicon substrate at a deposition angle of 85°.[11] Immediately after GLAD growth, the sample was transferred to a custom-built CVD system.[14] For the CVD process, acetylene was used as the hydrocarbon precursor due to its ability to decompose to graphene at low temperatures, which is shown schematically in Fig. 1(a). During the deposition, the temperature was raised to 350 °C under 3.4 mTorr of hydrogen; then, 3.0 mTorr of acetylene was added to the hydrogen, and the furnace was raised to 500 °C for 1 min. Under such conditions, the carbon solubility in cobalt is still significant, which results in a multilayer graphene product.[15] Additionally, it has been shown that graphene coatings grown at 350 °C can stabilize the nanopillar's morphology from thermal damage at temperatures up to 500 °C.[16] After the CVD process, the sample was characterized using angle-resolved GSE,[9] Raman spectroscopy, SEM, and TEM. GSE measurements were carried out in the spectral range from $\lambda = 400$ to 1650 nm using a commercial instrument equipped with an automated sample rotation stage (RC2, J.A. Woollam Co. Inc.). Mueller matrix data were obtained for four different angles of incidence $\Phi a = 45°$, 55°, 65°, and 75° for a complete in-plane sample rotation from $0° \leq \phi \leq 360°$ in steps of 6°.[9] In addition to the GSE measurements, unpolarized micro Raman scattering experiments were performed using a commercial Raman microscope (Thermo Scientific DXR) with a 532 nm laser and a 1 μm spatial resolution in order to assess the quality and morphology of the graphene grown on the 3D nanostructures. High-resolution cross-section SEM micrographs were obtained using a Hitachi S4700 field emission SEM. TEM images were obtained using a FEI Tecnai Osiris transmission electron microscope.

Figure 1 depicts the cross-section SEM micrographs of the Co SCTF sample before (b) and after (c) the graphene CVD. The 3D nanostructure geometry remains intact after the graphene CVD process, having been protected from melting by an intermediate carbon coating. As can be inferred from Figs. 1(b) and 1(c), a slight decrease of the slanting angle from 60.0° to 54.2° occurs. Additionally, as shown in Fig. 1(d), the average diameter of the nanopillars increase from 20 to 31 nm, suggesting growth of a several-nanometer thick graphene layer. Note that control experiments carried out without introducing the hydrocarbon precursor resulted in damage to the morphology of the nanostructures. The slanting angle change is tentatively associated with the acetylene decomposition on the Co surface, in particular, at the interface of the nanocolumns and the Si substrates.

The Raman spectroscopy data obtained after graphene deposition are presented in the inset of Fig. 2. Three distinct

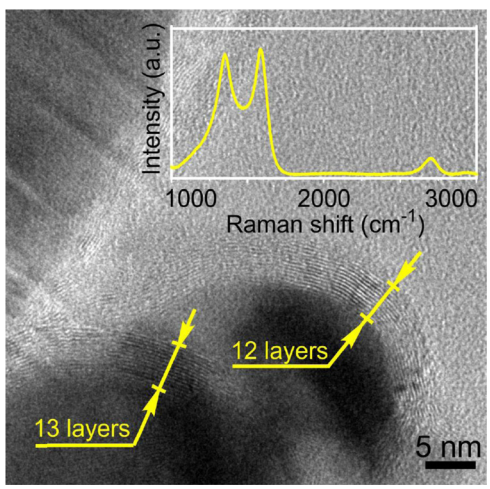

FIG. 2. Experimental TEM image of multilayered graphene product coating the tips of the cobalt nanopillars. Inset shows the Raman spectrum obtained from the Co SCTF after the graphene CVD. Three distinct Raman bands are identified as D-, G-, and 2D-band around 1300, 1600, and 2700 cm^{-1}, respectively.

Raman bands identified as D-, G-, and 2D-bands can be observed.[17] The Raman spectrum for the graphene-coated Co SCTFs resembles neither typical monolayer nor multilayer graphene Raman data nor does it show the fingerprints of graphite.[17,18] The presence of carbon nanotubes can be ruled out based on the fact that resonances typical for carbon nanotube Raman spectra, e.g., the splitting of the G-band, do not occur here.[19]

The comparatively strong Raman D-band ($I_D/I_G = 0.921$) is typically indicative for the presence of structural defects.[17,20] Nevertheless, this observation is not surprising due to the fact that the graphene layers are warped around the Co nanorods with an average diameter of roughly 20 nm. Furthermore, TEM imaging in Fig. 2 shows that the graphene layers conformally coat the tips of the nanorods which gives rise to curvature necessitating inclusion of rings of non-hexagonal symmetry.

The resonance observed at $\omega_{2D} = 2697 \pm 1\,\mathrm{cm}^{-1}$ is attributed to the second order D-band contribution. It is well known that the Raman 2D-band is particularly sensitive to the number of graphene layers and is furthermore closely correlated with the electronic band structure of the material.[17,19,20] For single-layer graphene, the 2D resonance is located at $\omega_{2D} = 2685 \pm 1\,\mathrm{cm}^{-1}$. With the increase in number of graphene layers, the 2D resonance shifts to higher energies and can be observed for graphite as a composition of two contributions at $\omega_{2D,1} \approx 2720\,\mathrm{cm}^{-1}$ and $\omega_{2D,2} \approx 2740\,\mathrm{cm}^{-1}$.[21] Additionally, the relatively low value for the I_{2D}/I_G ratio of 0.126 indicates that the product primarily consists of several-layer graphene. This is consistent with the data gathered by TEM, which shows that the Co nanopillars are conformally coated with 12–13 graphitic layers. We therefore conclude that the CVD process here described resulted in graphene with more than 10 layers and substantial structural disorder, which is attributed to the 3D nanostructured surface.

Angle-resolved GSE data determine structural and anisotropic optical properties of the Co SCTF before and after the CVD process. It has been demonstrated that the permittivity tensor of highly spatially coherent slanted nanocolumns can be accurately described from THz frequencies to the ultraviolet using an anisotropic Bruggeman effective medium approximation (AB-EMA).[12,13,22] In order to correctly render the optical response of the SCTFs discussed here, the Bruggeman approximation, which was developed for disordered inhomogeneous media with spherical inclusions,[23] is augmented to account for highly spatially coherent, oriented elliptical inclusions.[10,12,24–26] The effective dielectric function tensor described by the AB-EMA is composed of three major components $\varepsilon_{eff,a}$, $\varepsilon_{eff,b}$, and $\varepsilon_{eff,c}$ along the major axes a, b, and c of an orthorhombic system. $\varepsilon_{eff,j}$ with $j = a$, b, and c given in implicit form by[12,27]

$$\sum_{n=1}^{m} f_n \frac{\varepsilon_n - \varepsilon_{eff,j}}{\varepsilon_{eff,j} + L_j(\varepsilon_n - \varepsilon_{eff,j})} = 0\,. \tag{1}$$

In Eq. (1), the material constituents' dielectric permittivity and volume fraction are denoted by ε_n and f_n, respectively. For the as-grown Co SCTF, the corresponding AB-EMA consists of two material contributions: the permittivity of the host medium (air) $\varepsilon_1 = 1$ and the permittivity of the nanorods (cobalt) ε_2. In the case of the post-CVD SCTFs, the graphene permittivity is included in the AB-EMA as a third component ε_3. The factors L_j render the depolarization of the elliptical inclusions along the major polarizability axes a, b, c independent of the ellipsoid shape where the sum-rule $L_a + L_b + L_c = 1$ must be satisfied.[28] The collective response of slanted nanocolumnar arrays may exhibit quasi-monoclinic properties.[9–11,13] Such an effect is described through projection of the orthogonal basis system onto the monoclinic in which the semiaxis b is tilted towards c by a monoclinic angle β as described in Ref. 10 and 12.

The angle-resolved GSE data sets for each sample were combined within a common model data analysis during which model parameters (see Table I) were varied using least-squares approaches, which minimize a weighted test function until calculated and measured data match as close as possible (best-model). A good agreement between the experimental and best-model calculated Mueller matrix data is found using a three-phase stratified layer optical model composed of Si substrate, native SiO_2 layer, and AB-EMA based layer for the SCTF. The best-model parameters obtained for both samples are summarized in Table I. Literature values were used for the dielectric function of Si substrate, SiO_2, and CVD graphene and which were not further varied during the analysis. The dielectric function of the cobalt nanorods was varied during the analysis wavelength-by-wavelength to account for differences between bulk cobalt permittivity and GLAD-grown material.[12] The obtained results are comparable to those reported earlier.[11] The AB-EMA model for the graphene-coated SCTFs were geometrically correlated with the fit parameters obtained by the as-grown model. In particular, it was inferred that the ratio between volume fraction of cobalt and thickness of the film is to be constant, and also that the change in thickness induced by CVD is directly related to the change in the slanting angle of the pillars. It is worth noting in passing that, when these geometrical constraints were not imposed on the AB-EMA model for the graphene-coated SCTFs, the best fit parameters only differed from the geometrically-corrected parameters by approximately 3%. This suggests that knowledge of the as-grown fit parameters, though helpful, are not necessary to obtain a good fit for the graphene-coated SCTFs.

Figure 3 depicts the experimental (symbols) and best-model calculated (solid lines) Mueller matrix data obtained

TABLE I. Summary of the best-model parameters obtained from the analysis of the angle-resolved GSE data obtained before (Fig. 3(a)) and after graphene CVD (Fig. 3(b)). The uncertainty of the last digit (90% reliability) is given in parentheses.

Parameter		As-Grown	Post-CVD
Thickness	d (nm)	80.80(4)	94.81(0)
Slanting angle	θ (°)	60.0(2)	54.1(6)
Volume fraction	f_{void} (%)	78.3(4)	71.3(2)
	f_{MLG} (%)	N/A	10.5(7)
Monoclinic angle	β (%)	83.8(7)	87.1(4)
Depolarization	L_a	0.3833(5)	0.4261(3)
	L_b	0.4909(7)	0.4375(8)
	L_c	0.1256(8)	0.1362(9)

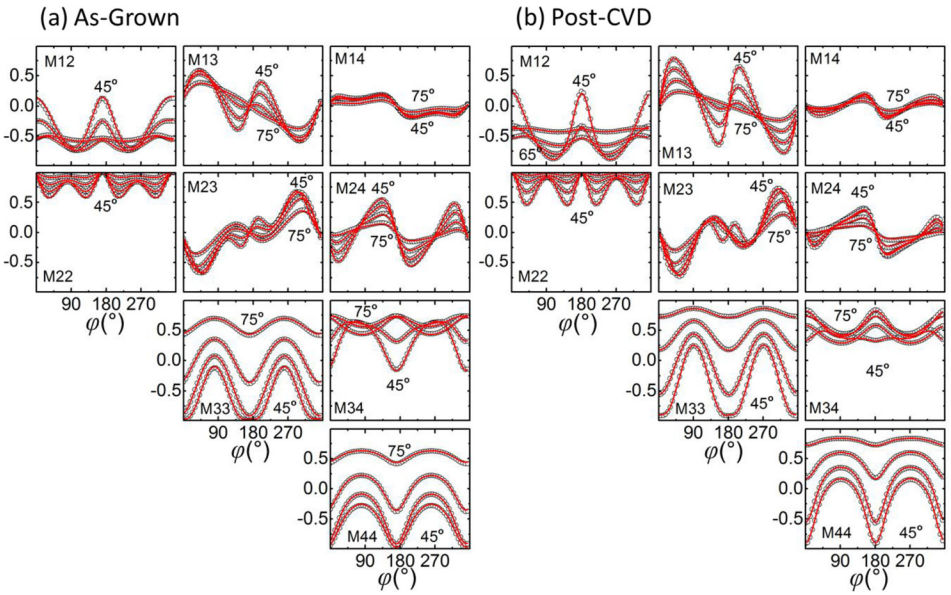

FIG. 3. Experimental (circles) and best-match calculated (solid lines) GSE data of the (a) as-grown GLAD Co SCTF (Fig. 1(b)) and (b) the same SCTF after graphene CVD (Fig. 1(c)) as a function of the sample azimuth angle φ shown exemplarily for $\lambda = 500$ nm at three different angles of incidence $\Phi_a = 45°$, 55°, 65°, and 75°. Note that elements M_{21}, M_{31}, M_{32}, M_{41}, M_{42}, and M_{43} are omitted as they are antisymmetrically equivalent to M_{12}, M_{13}, etc.

for the Co SCTF before (Fig. 3(a)) and after graphene deposition (Fig. 3(b)) as a function of the sample in-plane orientation ϕ. Comparing the GSE spectra obtained before and after the graphene CVD, it can be observed that the so-called off-diagonal block Mueller matrix elements (M_{13}, M_{14}, M_{23}, M_{24}) are subject to change whereas the on-diagonal Mueller matrix (M_{12}, M_{22}, M_{33}, M_{34}) components only scale slightly in their amplitude. This observation is also reflected in the effective optical constants of the SCTF before and after graphene CVD, which are depicted in Fig. 4. The conformal graphene coating introduces the strongest changes on the polarizability in a and b direction, while the c direction is only slightly shifted. While the as-grown SCTF exhibits biaxial optical properties, the graphene coating changes the optical properties of the SCTF to uniaxial.

This can be accounted for by looking at the relative changes in the a and b axes resulting from the geometric changes to the SCTFs. Assuming a close-packed arrangement of nanopillars on the surface of the substrate, the a and b axes are given by

$$a = \sin(30°) \tag{2}$$

and

$$b = \cos(30°) \cdot \cos(\theta), \tag{3}$$

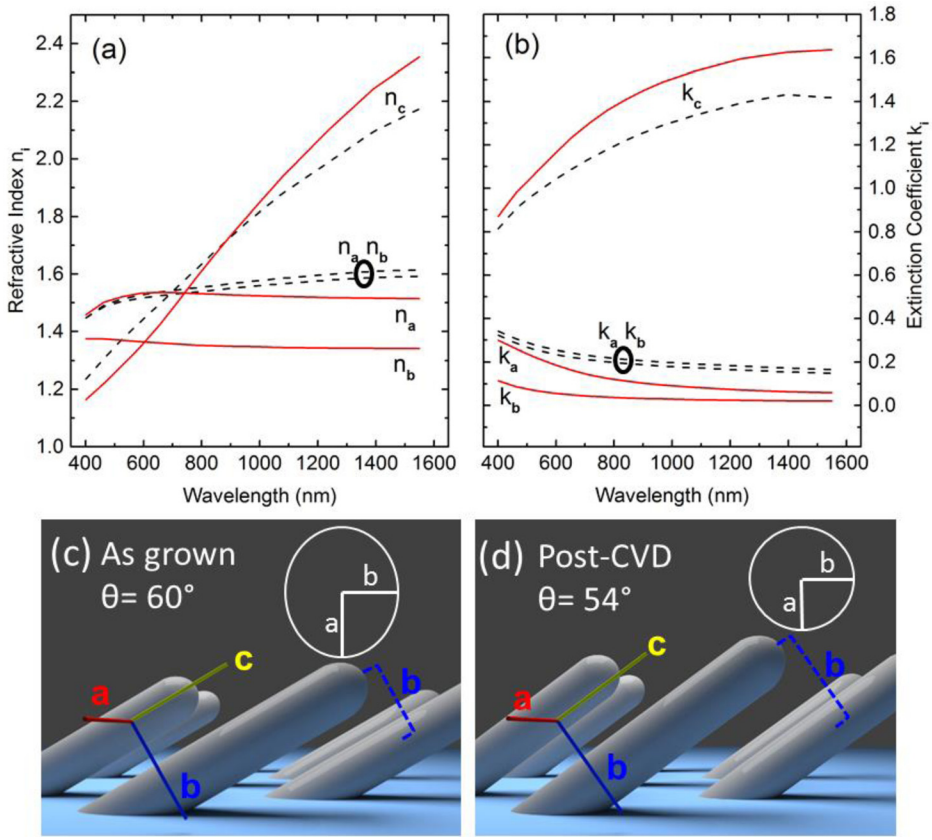

FIG. 4. (a) and (b) Best-model effective optical constants, (a) refractive index and (b) extinction coefficient, along major axes of polarizability a, b, and c for the as-grown Co SCTF (solid lines) in comparison to the post-CVD sample (dashed lines). (c) and (d) Schematic representations of magnitude of the b axis in (c) as-grown and (d) graphene-coated SCTFs. Insets show cross-sections along a and b axes of ellipsoid generated by major polarization axes. Note that the graphene coating renders the optical response of the sample uniaxial, i.e., the difference in the optical constants along a and b direction vanishes after the graphene growth due to the change in slanting angle as shown schematically in (c) and (d).

respectively, when normalized by the interpillar distance. Thus, changes to the slanting angle θ results in changes to the ratio between the *a* and *b* axes. When the slanting angle is 60.0°, the geometrically calculated *a* to *b* ratio is 0.866, which is consistent with its biaxial optical properties. However, when the slanting angle goes to 54.2°, the *a* to *b* ratio rises to 1.018. This is in excellent agreement with the ratio of 1.027 obtained by taking the ratio of the reciprocal of the *a* and *b* depolarization factors. Thus, the transition from biaxial to uniaxial can be accounted for by calculating the changes in the interpillar distances in the *a* and *b* directions incurred by changing slanting angles obtained from the AB-EMA method. This transition is demonstrated schematically in Figs. 4(c) and 4(d). It is worth noting that previous studies showed that the coating of Co nanopillars with a comparable thickness of Al_2O_3 by atomic layer deposition did not significantly change the biaxial nature of the materials' optical response and the *a* and *b* axes remained distinct.[12]

A very good agreement can be found for the structural parameters obtained by SEM, TEM, Raman, and GSE experiments. In particular, slanting angle and SCTF thickness agree very well between SEM and GSE best-model parameters (Table I). Assuming ideal cylindric nanocolumns with a diameter of 20 nm (Fig. 1), the AB-EMA graphene fraction (f_{MLG}) could correspond to a conformal coating with a thickness of 3.9 nm (about 13 ML), which would be in excellent agreement with the 12 to 13 ML estimated from the Raman and TEM measurements. We therefore conclude that the Co pillars were conformally coated with multilayer graphene based on GSE and Raman analysis.

In summary, it has been demonstrated that metal SCTFs can be conformally coated with graphene using a low-temperature CVD process and acetylene as a carbon supplying precursor gas. The low-temperature CVD process has been found to preserve the nanostructure integrity, suggesting that this process may be suitable for coating other cobalt nanostructures.[26,29,30] The structural parameters obtained by GSE, Raman spectroscopy, SEM, and TEM are in very good agreement. In particular, it has been shown that the anisotropic optical response can be accurately described using the AB-EMA approach where structural parameters, such as thickness, slanting angle, and graphene layer thickness (through graphene volume fraction) of graphene-coated cobalt SCTFs could be extracted with excellent accuracy. The methodology developed in this work will be useful for the synthesis and characterization of other graphene-coated 3D metallic nanostructures.

This work was supported by the National Science Foundation (NSF) through the Center for Nanohybrid Functional Materials (CNFM) (Grant No. EPS-1004094) and the Nebraska Materials Research Science and Engineering Center (MRSEC) (Grant No. DMR-1420645). Partial financial support from Army Research Office (W911NF-09-C-0097), NSF (DMR-0907475, ECCS-0846329), Nebraska Center for Energy Sciences Research (Grant No. 12-00-13), and J.A. Woollam Foundation is also acknowledged. This research was performed in part in Central Facilities of the Nebraska Center for Materials and Nanoscience (NCMN), which is supported by the Nebraska Research Initiative.

[1]T. Kasputis, M. Koenig, D. Schmidt, D. Sekora, K. B. Rodenhausen, K. J. Eichhorn, P. Uhlmann, E. Schubert, A. K. Pannier, M. Schubert, and M. Stamm, J. Phys. Chem. C **117**(27), 13971 (2013).
[2]K. B. Rodenhausen, D. Schmidt, T. Kasputis, A. K. Pannier, E. Schubert, and M. Schubert, Opt. Express **20**(5), 5419 (2012).
[3]J. S. Bunch, A. M. van der Zande, S. S. Verbridge, I. W. Frank, D. M. Tanenbaum, J. M. Parpia, H. G. Craighead, and P. L. McEuen, Science **315**(5811), 490 (2007).
[4]C. Lee, X. D. Wei, J. W. Kysar, and J. Hone, Science **321**(5887), 385 (2008).
[5]S. S. Chen, L. Brown, M. Levendorf, W. W. Cai, S. Y. Ju, J. Edgeworth, X. S. Li, C. W. Magnuson, A. Velamakanni, R. D. Piner, J. Y. Kang, J. Park, and R. S. Ruoff, ACS Nano **5**(2), 1321 (2011).
[6]D. Prasai, J. C. Tuberquia, R. R. Harl, G. K. Jennings, and K. I. Bolotin, ACS Nano **6**(2), 1102 (2012).
[7]D. B. Farmer, R. Golizadeh-Mojarad, V. Perebeinos, Y. M. Lin, G. S. Tulevski, J. C. Tsang, and P. Avouris, Nano Lett. **9**(1), 388 (2009).
[8]A. Sinitskii, A. Dimiev, D. A. Corley, A. A. Fursina, D. V. Kosynkin, and J. M. Tour, ACS Nano **4**(4), 1949 (2010).
[9]D. Schmidt, B. Booso, T. Hofmann, E. Schubert, A. Sarangan, and M. Schubert, Opt. Lett. **34**(7), 992 (2009).
[10]D. Schmidt, B. Booso, T. Hofmann, E. Schubert, A. Sarangan, and M. Schubert, Appl. Phys. Lett. **94**(1), 011914 (2009).
[11]D. Schmidt, A. C. Kjerstad, T. Hofmann, R. Skomski, E. Schubert, and M. Schubert, J. Appl. Phys. **105**(11), 113508 (2009).
[12]D. Schmidt, E. Schubert, and M. Schubert, Appl. Phys. Lett. **100**(1), 011912 (2012).
[13]D. Schmidt and M. Schubert, J. Appl. Phys. **114**(8), 083510 (2013).
[14]P. M. Wilson, G. N. Mbah, T. G. Smith, D. Schmidt, R. Y. Lai, T. Hofmann, and A. Sinitskii, J. Mater. Chem. C **2**(10), 1879 (2014).
[15]X. S. Li, W. W. Cai, L. Colombo, and R. S. Ruoff, Nano Lett. **9**(12), 4268 (2009).
[16]P. M. Wilson, A. Zobel, A. Lipatov, E. Schubert, T. Hofmann, and A. Sinitskii, ACS Appl. Mater. Inter. **7**(5), 2987 (2015).
[17]A. C. Ferrari and D. M. Basko, Nat. Nanotechnol. **8**(4), 235 (2013).
[18]A. C. Ferrari, J. C. Meyer, V. Scardaci, C. Casiraghi, M. Lazzeri, F. Mauri, S. Piscanec, D. Jiang, K. S. Novoselov, S. Roth, and A. K. Geim, Phys. Rev. Lett. **97**(18), 187401 (2006).
[19]A. C. Ferrari, Solid State Commun. **143**(1–2), 47 (2007).
[20]D. Yoon, H. Moon, H. Cheong, J. S. Choi, J. A. Choi, and B. H. Park, J. Korean Phys. Soc. **55**(3), 1299 (2009).
[21]R. P. Vidano, D. B. Fischbach, L. J. Willis, and T. M. Loehr, Solid State Commun. **39**(2), 341 (1981).
[22]T. Hofmann, D. Schmidt, A. Boosalis, P. Kuhne, R. Skomski, C. M. Herzinger, J. A. Woollam, M. Schubert, and E. Schubert, Appl. Phys. Lett. **99**(8), 081903 (2011).
[23]D. A. G. Bruggeman, Ann. Phys.-Berlin **416**(7), 636 (1935).
[24]D. E. Aspnes, Thin Solid Films **89**(3), 249 (1982).
[25]G. B. Smith, Opt. Commun. **71**(5), 279 (1989).
[26]A. P. Chumakov, S. V. Grigoriev, N. A. Grigoryeva, K. S. Napolskii, I. V. Roslyakov, A. A. Eliseev, A. I. Okorokov, and H. Eckerlebe, J. Phys. Conf. Ser. **247**, 012033 (2010).
[27]B. C. Bergner, T. A. Germer, and T. J. Suleski, J. Opt. Soc. Am. A **27**(5), 1083 (2010).
[28]A. H. Shivola, *Electromagnetic Mixing Formulas and Applications* (The Institution of Engineering and Technology, London, 1999).
[29]N. B. Chaure, P. Stamenov, F. M. F. Rhen, and J. M. D. Coey, J. Magn. Magn. Mater **290**, 1210 (2005).
[30]L. Serrano-Ramon, R. Cordoba, L. A. Rodriguez, C. Magen, E. Snoeck, C. Gatel, I. Serrano, M. R. Ibarra, and J. M. De Teresa, ACS Nano **5**(10), 7781 (2011).